Structural studies of hydrated samples of amorphous calcium phosphate and phosphoprotein nanoclusters

Samuel Lenton[a,b], Tommy Nylander[c], Carl Holt[d], Lindsay Sawyer[e], Michael Haertlein[b], Harrald Müller[f], Susana C.M. Teixeira[a,b]*

[a]EPSAM, Keele University, Staffordshire, ST5 5BG, UK. [b]Institut Laue–Langevin, 71 avenue des Martyrs, 38042 Grenoble cedex 9, France. [c]Dep. Chemistry, Division of Physical Chemistry, Lund University, P.O. Box 124, S-221 00 Lund, Sweden. [d]Institute of Molecular, Cell and Systems Biology, University of Glasgow, Glasgow G12 8QQ, UK. [e]Structural Biochemistry Group, Michael Swann Building, The King's Buildings, University of Edinburgh, Mayfield Road, Edinburgh EH9 3JR, Scotland. [f]European Synchrotron Radiation Facility, CS 40220, 38043 Grenoble, France. *Corresponding author: Susana C.M. Teixeira, Tel. +33(0)675135513. Email: teixeira@ill.fr

Abstract

There are abundant examples of nanoclusters and inorganic microcrystals in biology. Their study under physiologically relevant conditions remains challenging due to their instability, the requirements of sample preparation and other intrinsic limitations of the techniques used. Advantages of using neutron diffraction and contrast matching to characterize biomaterials are highlighted in this article. We have applied these methods and complementary techniques to search for long-range order within nanoclusters of calcium phosphate sequestered by bovine phosphopeptides, derived from osteopontin or casein. Hydrated and dried samples with different nanocluster radii were analyzed and compared to samples of known calcium phosphate phases. The absence of a distinct diffraction pattern from the nanoclusters is consistent with the presence of amorphous calcium phosphate structure.

Keywords

Biomineralisation, amorphous calcium phosphate, neutron diffraction, phosphoproteins, osteopontin, casein

Acknowledgments

At the Institut Laue Langevin (ILL) we would like to thank B. Demé, G. Zaccai, J. Rodriguez-Carvajal, H. Fischer and D. Richard for valuable discussions. We acknowledge the Grenoble European Molecular Biology Laboratory (H. Belrhali in particular) for access to in-house X-ray facilities, and the European Synchrotron Radiation Facility Chemistry Laboratory. We are very grateful to the Large Scale Structures and Life Sciences groups at the ILL for access to the facilities and general support. SL and SCMT would like to thank Keele University (Institute for the Environmental, Physical Sciences and Applied Mathematics, EPSAM), the ILL and Lund University for financial support. TN would like to acknowledge the Swedish Research Council. We are very grateful to the ILL for neutron beamtime.

1. INTRODUCTION

Loss of structural order can be caused by mechanical stress (Garcia et al. 1991), pressure effects (Hibi et al. 1993) or thermal treatment (Yang et al. 2003). Dehydration can also lead to an increase in disorder and can inhibit crystallization or recrystallization (Brindly et al. 1963). Loss of water within granular regions of starch, for example, was shown to be responsible for a loss of plasticity that precludes periodicity over larger scales (Perry and Donald 2000). Sample preparation requirements are a particular concern when studying biomaterials, which tend to be inhomogeneous on almost any length scale (for a review of structural hierarchies see Fratzl and Weinkamer 2007).

Electron (Egerton and Malac 2004) and synchrotron-based X-ray beams are often used to probe wide ranges of structural information. By combining, for instance, small and wide-angle X-ray scattering techniques it is possible to probe nm to μm length scales (Garcia et al. 1991, Paris 2008). High-energy irradiation is however known to induce damage to crystallinity (Kantoglu and Guven 2002), particularly when ordered water is present (Bursill et al. 1980). The non-destructive nature of neutron diffraction is extremely advantageous in this context. Dry or hydrated samples can be measured at room temperature so that the potential effects of drying, cryoprotectants and cryocooling can be eliminated. In addition, deuterium labelling can be used to decrease incoherent neutron scattering and to highlight specific parts of multicomponent macromolecular systems through contrast matching. An important caveat in the latter is the possibility that the structure can be perturbed by the use of D_2O or isotope labeling (see for example Liu et al. 2007), which underlines the need to use complementary techniques such as X-ray diffraction to test conclusions from neutron experiments.

Calcium orthophosphates are an integral structural component of a range of biomaterials, present in different phases and particularly relevant to oral biology, dentistry and medicine (Cai and Tang 2008, Skrtic et al. 2003). Crystals of carbonated hydroxyapatite are found in bones and teeth. Biphasic calcium phosphates of hydroxyapatite (Ca/P = 1.67) and β-tricalcium phosphate (TCP, $Ca_3(PO_4)_2$) show high bioactivity and osteoconductivity (Lee et al. 2013). Nanocrystalline apatites have biomineralisation and orthopaedic applications, yet the conditions of their formation and maturation remain poorly understood. Previous studies (Rey et al. 2007) showed the presence of a hydrated structured layer at the surface of nanocrystalline apatites, through which larger crystals can be formed. It was suggested this surface layer, which can be irreversibly altered by drying, confers unexpected properties *in vivo* and could be used to obtain bioactive coatings from nanocrystals.

Most vertebrate bodily fluids are supersaturated with respect to both hydroxyapatite and amorphous calcium phosphate (ACP), where some intrinsically disordered proteins such as caseins and osteopontin (OPN) form stable or metastable complexes with calcium phosphate (Holt et al. 2014, George and Veis 2008). The best characterised example is the casein micelle of milk, which contains hundreds of nanoclusters of calcium phosphate in a single colloidal casein micelle of ~100 nm radius (see also section 2.2). Clusters of 3 or more phosphorylated residues (phosphate centers) in the phosphopeptide chains bind electrostatically to a core of calcium phosphate, while the flanking sequences form a shell or corona around it (Bruyn et al. 2013, Clegg and Holt 2009). At equilibrium, the resulting calcium phosphate nanoclusters (CPN) have well defined average diameters in aqueous solutions, depending upon the properties of the sequestering peptide. For instance, core

radii of gyration of ~17.5 nm were observed for CPN complex with OPN 1-149 (Holt et al. 2014) and of ~1.85 nm for complexes with various casein phosphopeptides (Holt et al. 1998).

Interactions between proteins and crystals, including OPN peptides (Grohe et al. 2007), are central to many processes in biomineralisation. The inorganic core of dehydrated CPN samples has however been found to be amorphous, based on experimental results from a range of techniques including electron microscopy, X-ray diffraction, Fourier transform infrared spectroscopy (FTIR) and X-ray absorption spectroscopy (Cross et al. 2005; Holt et al. 1982, 1996 and 2009; Hunter et al. 1996; Holt and Hukins 1991). Drying or radiation damage could nonetheless destroy crystalline order in the CPN. It has been reported that biologically formed calcium phosphate precipitates form much smaller crystals than the naturally occurring geological counterparts: biological apatite crystals typically range from a few to hundreds of nanometers (Boskey 2003). Based on previous measurements of radii of gyration, the average diameter of a spherical CPN core sequestered by OPN 1-149 and β-casein 1-25 is ~45.2 nm and ~4.8 nm, respectively. Both core volumes are large enough to accommodate nanocrystallites of, for example, dicalcium phosphate dihydrate (DCPD, $CaHPO_4 \cdot 2H_2O$), octacalcium phosphate (OCP, $Ca_8H_2(PO_4)_6.5H_2O$) or hydroxyapatite (HA, $Ca_5(PO_4)_3OH$).

ACP can be prepared with a range of different Ca/P ratios (Zhao et al. 2011). Amorphous TCP (Ca/P = 1.5) is formed in alkaline conditions with a structure built by agglomeration of the so-called Posner clusters (Betts and Posner 1974, Blumenthal and Posner 1973): $Ca_9(PO_4)_6$ units of 0.8-1 nm diameter, where interstitial water can be removed irreversibly by drying (Kojima et al. 1994). This is an arrangement also present in

the unit cell of apatites, OCP and β-TCP. Hydrated ACP may mature into more crystalline forms through a process of solution and re-deposition (Blumenthal and Posner 1973, Kojima et al. 1994). It was reported that *in vitro* ACP maturation time is highly dependent on Ca/P ratio (Harries et al. 1987) as well as on pH. An acidic ACP that is prepared and kept under acidic conditions is unstable and tends to convert to crystalline DCPD (Combes and Rey 2010). The DCPD structure has water molecules sandwiched between corrugated sheets of calcium and hydrogen phosphate ions. It typically yields a characteristic diffraction spectrum with strong reflections arising from these sheets.

Previous studies have shown (Holt 2004, Holt et al. 1989) that the composition of micellar calcium phosphate is consistent with that of an acidic ACP. High-resolution electron microscopy (Lyster et al. 1984) of dried samples of micellar calcium phosphate showed that longer-range order did not extend over distances more than ~1.5 nm. This distance corresponds to the longest dimension of the DCPD crystalline unit cell. OCP has also been shown to hydrolyse into calcium-deficient apatites but it was shown that dehydration through a thermal treatment could cause a significant decrease in crystallite size (Neslon and McLean 1984). Both OCP (McGann et al. 1983) and DCPD can be *in vitro* precursors of HA (Nudelman et al. 2012, Addadi et al. 2012) but have only rarely been detected in mineralised tissue. They are, however, common in pathological calcifications such as dental calculi, urinary stones and chondrocalcinoses (Cheng 1991), formed at lower pH.

In summary, a range of factors can affect the formation and stability of calcium phosphate phases. Neutron diffraction is a powerful technique in the study of amorphous biomaterials or pharmaceuticals (Sarsfield et al., 2006). Here we used the q-range

available at the D16 neutron diffractometer of the Institut Laue-Langevin to study the structure of hydrated synthetic calcium phosphate, and CPN samples prepared in the laboratory and obtained from bovine milk. Our goal was to probe for periodic distributions of molecules in the calcium phosphates. Although insensitive to shorter-range order such as the Posner clusters, the D16 neutron diffractometer allows for long-range order (see for example Carriere et al. 2009) to be detected in wet pellets and at room temperature. Importantly, in the context of biological structures, the relatively long neutron wavelength allows for contrast matching studies, which can be used to exclude contributions to scattering and diffraction from phosphopeptide structures such as protein fibrils (Thorn et al. 2005).

2. MATERIALS AND METHODS

2.1. Preparation of calcium phosphate nanoclusters sequestered by osteopontin phosphopeptides

In milk, OPN undergoes proteolytic processing by several different proteases, leading to a mixture (OPNmix) of different phosphopeptides (Holt and Hukins 1991, Holt et al. 1989). Naturally occurring OPNmix was isolated from bovine milk as previously described (Holt et al. 2009). The principal components are N-terminal peptides ending between residues 145 and 153 of the mature protein sequence (Christensen and Sorensen 2014). Previously this group of N-terminal peptides (Holt et al. 2009) was considered equivalent to OPN 1-149. We have kept this nomenclature here for the sake of simplicity and continuity.

OPNmix CPN were prepared by the simple mixing method to give final concentrations of 22 mM calcium, 20 mM inorganic phosphate, an ionic strength of 63 mM

and pH 7.0 (Holt et al. 2009). At equilibrium, the solution has a free calcium ion concentration of 0.5 mM and, on average, each peptide is attached to the calcium phosphate nanoclusters core through only one of its three phosphate centers. Samples were allowed to equilibrate for at least 14 days prior to centrifugation.

The stability of OPNmix CPN even at high ratios of D_2O (Holt et al. 2014) allowed for the use of samples prepared in 41% and 100% D_2O solutions. The 41% D_2O contrast was chosen to match out potential contributions from the phosphopeptide (Holt et al. 1998), but this intermediate percentage of D_2O is also useful in the assignment of peaks in the FTIR spectra. The 100% D_2O solutions were used for maximum signal-to-noise ratio. Two hydrated samples were produced from solutions of 10 ml of 30 mg/ml OPNmix CPN using 41% D_2O or 100% D_2O. Both solutions were centrifuged at 85000 g for 16 h, yielding hydrated pellets that were stored at 8 °C.

The same protocol was used to produce a dried OPNmix CPN sample from an H_2O solution for comparison, with an extra lyophilizing step. The sample was left overnight in a desiccator over silica gel, and stored at 4°C.

2.2. Preparation of micellar calcium phosphate

A concentrated form of the calcium phosphate, known as micellar calcium phosphate, can be recovered from a proteolytic digest of the casein micelles and has been shown to contain the most highly phosphorylated casein subsequences (Ono et al. 1994; Holt et al. 1986). The preparation of a hydrated sample of micellar calcium phosphate was based on protocols previously described (Holt et al. 1986). The casein micelle substructure and size are however slightly changed when H_2O is replaced by D_2O (Nelson and McLean 1984,

McGann et al. 1983) and for this reason the pronase digested sample was only produced in H_2O.

Casein micelles were pelleted in six tubes by centrifuging 240 ml of skim milk (1.5mM sodium azide were included in all milk solutions) at 60000 g for 1 h. The supernatants were discarded and the pellets redistributed into two tubes, refilled with more skim milk and redispersed by stirring for 24 h. 1 ml of a solution containing 200 µg of a broad specificity proteinase (Pronase, 81748 *Fluka*) was added after dispersion. The solution was placed in a Visking tube and dialysed at room temperature against 3 liters of skimmed milk, with stirring, for 24 h. During dialysis, the milky white solution clarified as the casein peptides were digested. A clear brown pellet was recovered from the optically clear digested solution by centrifugation (85 000 g for 16 hours at 8°C). Previous work (Ono et al. 1994, Holt et al.1986) has shown that the pelleted micellar calcium phosphate comprises calcium phosphate nanoclusters and casein phosphopeptides resistant to proteolytic digestion.

2.3. Preparation of calcium phosphate samples

An ACP sample was prepared as described previously (Holt et al. 1986), by rapid mixing at room temperature, with stirring, of 500 ml of a phosphate solution with 500 ml of a calcium solution. The phosphate solution had the composition 100 mM NaH_2PO_4 and 100 mM Na_2HPO_4, whereas the calcium solution had the composition 4 mM $CaCl_2$, 135 mM NaCl, 14 mM $MgCl_2$ and ~10 µg of a tryptic phosphopeptide mixture, prepared from whole casein and purified essentially as described previously (Reynolds et al. 1994). It was added to the calcium solution to inhibit the maturation of the ACP into crystalline phases.

At this low concentration of the casein phosphopeptide it cannot sequester any significant fraction of calcium phosphate in the form of CPN. The pH was adjusted to 7.0 and maintained at this value by adding 0.4M NaOH with rapid stirring. The precipitate formed was collected by filtration through a Sartorius membrane of 0.45μm porosity and freeze-dried. The dried powder, which can still include 10-20% of tightly bound water molecules (Zahid et al. 1985), was kept over silica gel overnight, before storage at -20°C.

Flat, plate-like, monoclinic crystals of DCPD were prepared using a published protocol (Miller et al. 2012). 0.825 g of KH_2PO_4 and 3.013 g of Na_2HPO_4 were dissolved in 700 ml of deionized water, followed by rapid addition, with stirring, of 200 ml of a solution containing 4.014 g of $CaCl_2{\cdot}2H_2O$. The solution was stirred for 80 min at room temperature to allow for complete precipitation. The solid was recovered by filtration, washed with deionised water and dried overnight at 37°C in a desiccator over silica gel. The powder was stored at -20°C.

2.4. Dynamic Light Scattering and Fourier transform Infrared spectroscopy

Formation of OPNmix CPN was demonstrated by dynamic light scattering measurements using a Malvern Zetasizer Nano S (Malvern Instruments Ltd., UK) at a scattering angle of 173°. The light source was a 4mW He-Ne laser operating at a wavelength of 633 nm. The sample was filtered through a *Whatman* filter with a 0.2 μm pore size and the correlation function recorded at 25°C, with at least 3 repeat measurements to check reproducibility.

FTIR spectra of the hydrated and dried CPN samples and the dry calcium phosphate samples were recorded before and after neutron diffraction experiments (Figures S1 and S2) with a Bruker VERTEX 70 Fourier transform infrared spectrometer equipped with a

diamond ATR device. Each spectrum was the average of 64 scans with a spectral resolution of 2 cm^{-1}. The spectra were recorded and stored using spectroscopic software (OPUS, Bruker Inc.).

2.5. Neutron and X-ray diffraction

Samples were analysed at room temperature over the q-range of 0.12-2.24 $Å^{-1}$ using the small momentum transfer neutron diffractometer D16, at the Institut Laue-Langevin (Grenoble, France). Exposure times of 30 min were used per angular 2θ step of 18.5°. The scattering wave vector q is a function of the wavelength λ (4.767Å, beam bandwidth $\Delta\lambda/\lambda$ = 1%) and the scattering angle (2θ), where $q=(4\pi/\lambda).\sin\theta$. A beam diameter of 3 mm was used (the divergence calculated directly from the image of an attenuated beam was 0.33°). The average flux on the sample was $1x10^6$ neutrons.cm^{-2}.s^{-1}. Data were recorded on a millimeter-resolution large area ^{3}He detector (MILAND; 320x320 mm^2). All samples were measured in spherically symmetric sealed sample containers of 5 mm diameter, for which the contribution was determined and subtracted from each of the sample diffraction scans.

Data collection was carried out for the OPNmix CPN samples (prepared in H_2O, D_2O and 41% D_2O) and pelleted after 3 weeks of maturation to ensure that the nanoclusters had reached their equilibrium size. The diffraction measurements were repeated 4 weeks later: no changes were observed in the corresponding diffraction patterns. While the hydrated samples were pelleted to obtain as high a concentration of the nanoclusters in the beam, the powder samples were loaded into the sample container without compaction. As a final control the ACP dry sample was exposed to ambient

humidity by leaving the sample container open at room temperature for ~3 extra weeks. Neutron diffraction data were recorded‡ for comparison (Fig. I). Data reduction was carried out using the Large Array Manipulation Program (LAMP; Richard et al. 1996) provided by the Institut Laue-Langevin.

X-ray diffraction data were collected on the same samples at room temperature over the q-range 0.31-3 $Å^{-1}$, using a GeniX Cu high flux generator. The average flux was ~400x10^6 photons.s^{-1} for a beam size at focus ~200x200 $μm^2$ with a divergence of 5 mrad. Data were recorded on a Mar345 detector with exposure times of 10 min per sample.

2.6. Simulated neutron and X-ray diffraction patterns

The minimum number, purity and size of crystallites needed for detection of their presence in the sample depend on a complex number of correlated sample and instrumental parameters. Recent studies (Fewster, 2014) have for example shown that dynamic and kinematic scattering must be taken into account to explain the high sensitivity of experimental powder diffraction data despite predictions of weak intensity measurements and low accuracies. Simulated neutron and X-ray diffraction patterns were obtained from the Institut Laue-Langevin's PHP-MySQL Inorganic Crystal Structure Database (ICSD-for-WWW; Supplementary material Fig. S3). These showed that the experimental 2θ ranges and wavelengths are appropriate to detect the various possible calcium phosphate crystal structures when large crystals are present.

Neutron diffraction powder patterns were also calculated using the FullProf suite (Rodriguez-Carvajal, 1993; Rodriguez-Carvajal, 2001) and high quality crystallographic information files for DCPD (ICSD-16132; Curry et al.,1971) and HA (ICSD-16742; Posner

et al., 1958). Simple single-line methods were used to account for size-strain broadening (Mittemeijer and Welzel, 2008). The need to avoid sample preparation bias precluded the addition of a known amount of an investigated standard to the samples. Taking this into consideration, as well as the relatively low resolution of the neutron data, an advanced analysis was not justified. Average spherical shapes were assumed for potential crystallites, defined by a diameter chosen to be compatible with the volumes of the inorganic core for OPNmix CPN and casein CPN. No super-cell calculations were used to include distortion effects.

3. RESULTS AND DISCUSSION

3.1. Dynamic light scattering

After 14 days the formed OPNmix-CPN had an intensity-averaged hydrodynamic radius of ~22.5 nm in solution (H_2O, 41% D_2O and 100% D_2O), as calculated from light scattering measurements,in agreement with previous findings (Holt et al., 2014; Holt et al, 2009). Light scattering measured both before and after pelleting (ultracentrifuged samples were re-suspended in their respective buffers) showed no significant changes.

3.2. Fourier Transform Infrared spectroscopy

FTIR spectra for the dried ACP and DCPD control samples are in close agreement with previously published results (Berry and Baddiel 1967, Trpkovska et al. 1999, Hirsch et al. 2014), as are the spectra for the CPN samples (see Supplementary Material Fig. S1 and Fig.S2).

3.3. Neutron and X-ray diffraction

ACP and DCPD neutron diffraction were directly measured as controls. The DCPD sample showed two clear diffraction peaks matching the expected pattern (Figure I). This is indicative of the sensitivity of the technique used, given peaks measured for DCPD have simulated intensities comparable to other calcium phosphate crystalline forms. For ACP no Bragg peaks were detected over the 2θ range measured (only peaks 15 times above the standard deviation were considered significant). ACP was however allowed to mature over a period of 3 weeks, exposed to humidity, and diffraction peaks were then detected in the angular ranges matching DCPD.

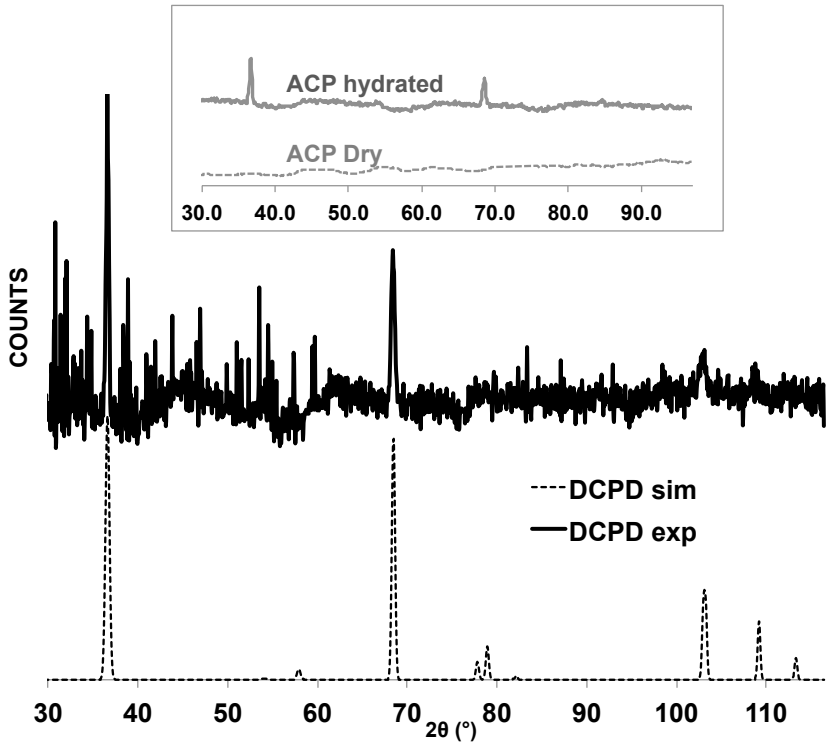

Figure I. Neutron diffraction pattern of the DCPD sample: a sharp Bragg peak was observed at a 2θ of 36.3° (I/σ)=20.9) and a second peak at 67.8° (I/σ=16.8; a similar intensity would be expected for a HA peak at 2θ of ~76°), matching the simulated pattern as shown (simulation based on the previously published crystal structure of DCPD; Curry and Jones, 1971). The inset shows an overlay of ACP diffraction patterns before and after maturation. Only the 2 peaks shown were distinguishable above the background.

The pronase digested casein sample was chosen to provide a comparison between CPN produced with different peptides, namely casein and OPN. None of CPN samples analyzed showed clear neutron diffraction peaks (Fig. II). CPN samples were analyzed by X-ray diffraction covering a 2θ range of 4-45°. For the OPNmix CPN sample in 41% D_2O, for which any protein contributions are matched out, the X-ray data provide a cross-validation of the neutron diffraction result. Figure IIb shows the results obtained for the CPN samples: the patterns are featureless, in agreement with the neutron diffraction data.

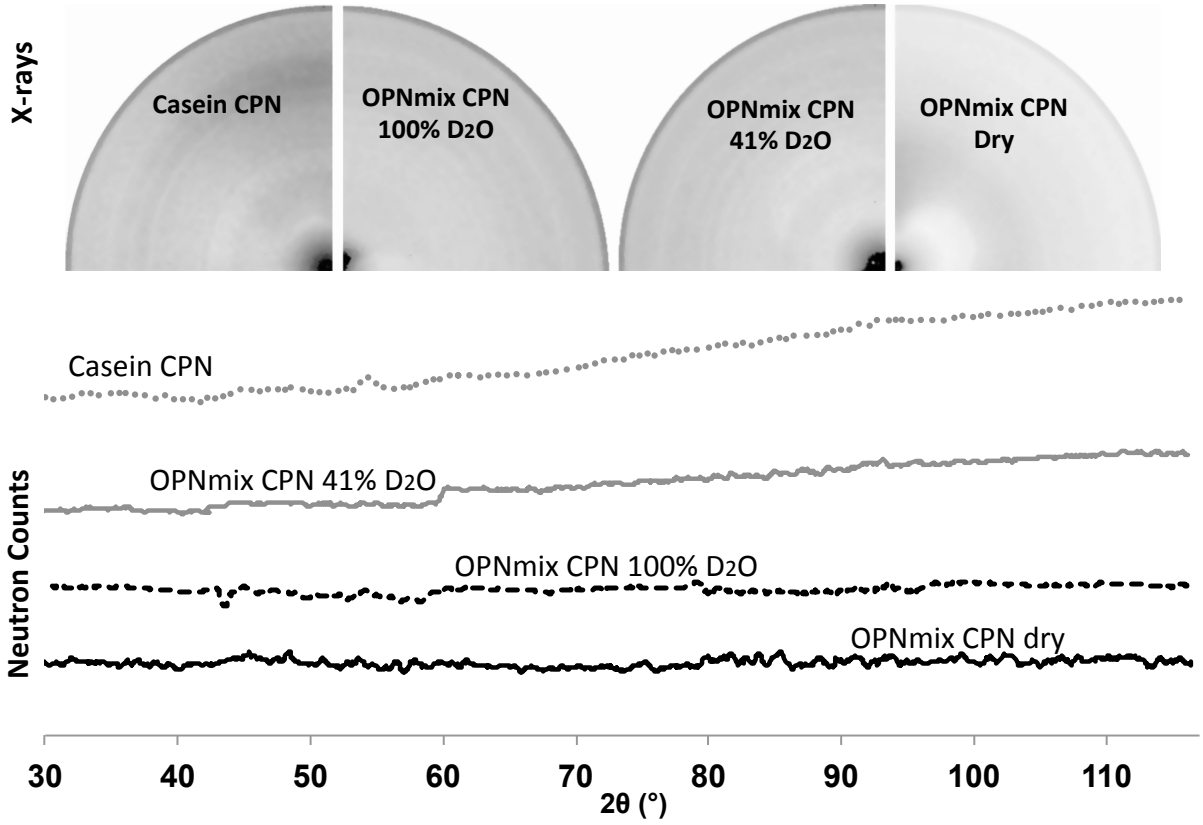

Figure II. The plot shows an overlay of the neutron diffraction patterns of the OPNmix and pronase digested CPN samples. Intensities are arbitrary. The patterns are similar to dry ACP, where no unambiguously identifiable diffraction rings are detected. The top insets show X-ray diffraction patterns for the CPN samples in the range of 2.07-20Å.

Figure III shows simulated neutron diffraction patterns of DCPD and HA for different possible sizes of crystallites, chosen to cover an illustrative range from a size equivalent to just one or two stacked unit cells, up to the full diameter of the core of CPN. DCPD and HA were chosen as representative potential structures that crystallise in small unit cells. If pure HA crystallites were present (Fig. IIIb), and given that the experiments carried out allowed for data to be collected up to a 2θ of 115°, the simulations suggest that crystallites of 18.9Å - large enough to include two or more unit cells stacked in the 'b' or 'c' unit cell edge directions - would cause a very broad peak centred at ~34°.

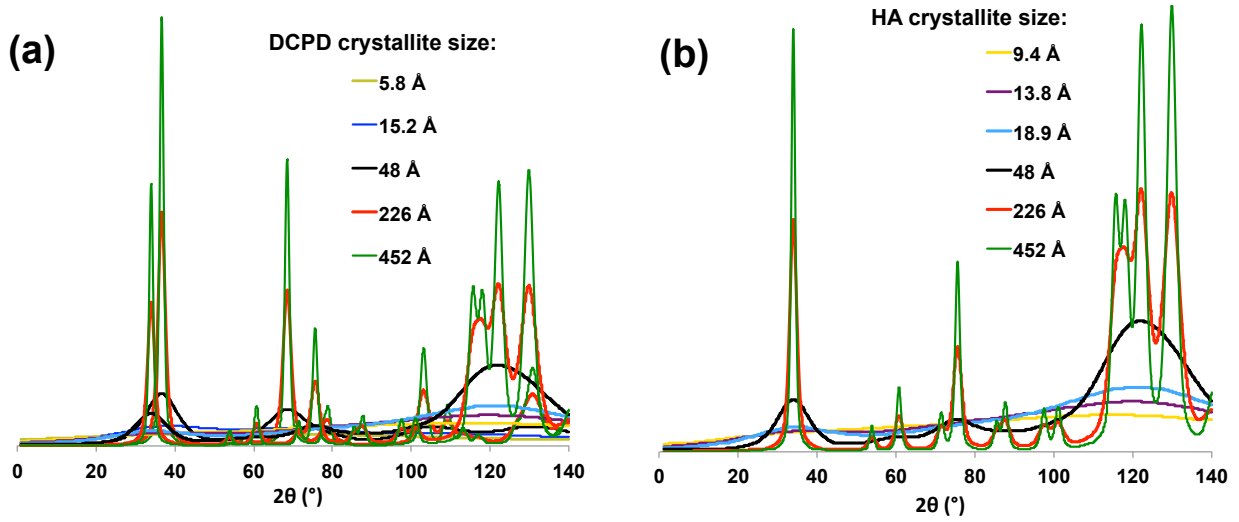

Figure III. Simulations of neutron diffraction at D16 for samples containing crystallites at different sizes assuming **(a)** pure DCPD crystals and **(b)** pure HA crystals. The DCPD unit cell assumed: a, b, c = 5.812, 15.18, 6.239 (Å), β = 116.43°; HA hexagonal unit cell: a, b = 9.432, c=6.881 (Å). The core of OPNmix CPN has a diameter of ~452Å (radius 226Å shown for comparison), while the core for casein CPN has a diameter of 48Å. The 2θ range shown includes data beyond the experimental angle measured on D16 but it is shown to highlight the peak tails that fall within the accessible range.

A second broad peak would be outside the experimental range but a tail would cause intensities to increase significantly with the scattering angle from a 2θ of 60°. A similar profile would already be expected for a 13.8Å crystallite, which can contain two unit cells stacked along the 'c' direction filling a significant volume of the casein CPN core, for

example. For DCPD, the simulations suggest that the experimental resolution would not allow detection of the presence of crystallites formed by up to 3 unit cells stacked in the 'a' direction, nor any made of a single monoclinic unit cell (as shown by the broad intensity profile for 5.8Å or 15.2Å).

4. CONCLUSION

A relatively dense packing of potential crystallites inside the CPN core is expected. The extra Gibbs free energy for nanocrystallite surfaces is significant and aggregation lowers the exposed interfacial surface area in an aqueous environment. The neutron diffraction patterns recorded did not however show any signs of homogeneous crystallites ≥18.9Å in the core of casein CPN or OPNmix CPN. The presence of heterogeneous mixtures of crystallites and mixtures of crystalline phases cannot however be excluded based solely on the results reported here. In particular as combined diffraction effects could flatten the diffraction signatures of the different crystal forms. The irreversible maturation of calcium phosphate to HA does occur through intermediates but given the consistency of the results at different times the presence of a mixture of crystalline forms in the inorganic core of CPN seems unlikely.

Compared to casein CPN, the larger OPNmix CPN core can be explained by higher levels of hydration at the central region, consistent for example with the presence of amorphous TCP. Previous studies (Heughebaert and Montel, 1982) have shown that hydrolysis of amorphous TCP can lead to the formation of HPO_4^{2-}, OH^- and a range of $Ca_9(PO_4)_{(6-x)}(HPO_4)_x(OH)$ compositions, an intermediate step before the formation of calcium deficient apatite. It is unclear if the CPN core traps such an intermediate state.

The lack of higher order structure in the core may be required for sequestration by the peptide and favor calcium bioavailability through higher kinetic solubility and rate of solution (amorphous phases lack the lattice energy of calcium phosphate crystals; Mahamid et al., 2010). Cross *et al (*2005) proposed a model of the inorganic core in casein CPN, consisting of two amorphous calcium phosphate phases: a central phase (Ca/P = 1.5), and a calcium-rich phase (Ca/P = 2) in direct contact with the peptide. It still however remains unclear how hydration affects the Ca/P ratios and the internal structure of the core.

It has previously been shown that the initial step of *in vivo* mineralization requires a highly amorphous precursor calcium phosphate that later matures into HA within the extracellular matrix (Mahamid et al. 2011), and a similar finding was observed in tooth enamel (Holt 1997). Collagen can be mineralized with HA by OPN CPN (Rodriguez et al., 2014). OPN and a similar phosphopeptide, bone sialoprotein, are distributed in bone and cementum (Nudelman et al., 2012; Rodriguez et al., 2014) suggesting activity as process directing agents delivering calcium phosphate to collagen fibrils. The amorphous and highly hydrated nature of OPN CPN would be consistent with this role.

References

Addadi L, Vidavsky N, Weiner S (2012). Transient precursor amorphous phases in biomineralization. In the footsteps of Heinz A. Lowenstam. *Z. Kristallogr.*, 227, 711–717.

Berry E, Baddiel C (1967). The infra-red spectrum of dicalcium phosphate dihydrate (brushite). *Spectrochim. Acta A: Molecular Spectroscopy*, 23, 2089–2097.

Betts F, Posner A (1974). An X-ray radial distribution study of amorphous calcium phosphate. *Mater. Res. Bull.*, 9, 353–60.

Blumenthal N, Posner A (1973). Hydroxyapatite: mechanism of formation and properties. *Calc. Tiss. Res.*, 13, 235-243.

Boskey A (2003). Bone mineral crystal size. *Osteoporosis Int.*, 14, S16.

Brindley G, Hayami R (1963). Kinetics and Mechanisms of Dehydration and Recrystallization of Serpentine—II, Spectrum of Activation Energies for Recrystallization. *Clays and Clay Minerals*, 12(1), 49-54.

Bursill L, Lodge E, Thomas I (1980). Zeolitic structures as revealed by high-resolution electron microscopy. Nature, 286,111-113.

Cai T, Tang R (2008). Calcium phosphate nanoparticles in biomineralization and biomaterials. *J. Mater. Chem*., 18, 3775–3787.

Carrière D, Belloni L, Demé B, Dubois M, Vautrin C, Meister A, Zemb T (2009). In-plane distribution in mixtures of cationic and anionic surfactants. *Soft Matter*, 5, 4983-4990.

Cheng P-T (1991). *Pathologic Mineralization in Humans, in Mechanisms and Phylogeny of Mineralization in Biological Systems*, Springer Japan, 241-245.

Christensen B, Sørensen ES (2014). Osteopontin is highly susceptible to cleavage in bovine milk and the proteolytic fragments bind the α(v) β(3)-integrin receptor. *J. Dairy Science*, 97, 136-146.

Clegg R, Holt C (2009). An *E. coli* over-expression system for multiply-phosphorylated proteins and its use in a study of calcium phosphate sequestration by novel recombinant phosphopeptides. *Protein expression and purification*, 67, 23–34.

Combes C, Rey C (2010). Amorphous calcium phosphates: Synthesis, properties and uses in biomaterials. *Acta Biomaterialia*, 6(9), 3362-3378.

Cross K, Huq N, Palamara J, Perich J, Reynolds E (2005). Physicochemical characterization of casein phosphopeptide-amorphous calcium phosphate nanocomplexes. *J. Biol. Chemistry*, 280, 15362–15379.

Curry N, Jones D (1971). Crystal structure of brushite, calcium hydrogen orthophosphate dihydrate: a neutron-diffraction investigation. *J. Chem. Soc. A: Inorganic, Physical, Theoretical*, 3725-3729.

De Bruyn J, Goiko M, Mozaffari M, Bator D, Dauphinee R (2013). Dynamic Light Scattering Study of Inhibition of Nucleation and Growth of Hydroxyapatite Crystals by Osteopontin. *PLoS ONE*, 8(2), e56764.

Egerton R, Malac P (2004). Radiation damage in the TEM and SEM. *Micron*, 35, 6, 399–409.

Fewster P (2014). A new theory for X-ray diffraction. *Acta Cryst A*, 70, 257-282.

Fratzl P, Weinkamer R (2007). Nature's hierarchical materials. *Progress in Materials Science*, 52, 1263-1334.

Garcia F, Abrio M, Rodriguez M (1991). Effects of dry grinding on two Kaolins of different degrees of crystallinity. *Clay Minerals*, 26, 5-565.

George A, Veis A (2008). Phosphorylated proteins and control over apatite nucleation, crystal growth, and inhibition. *Chem. Reviews,* 108, 4670–4693.

Grohe B, O'Young J, Ionescu D, Lajoie G, Rogers K, Karttunen M, Goldberg H, Hunter G (2007). Control of calcium oxalate crystal growth by face-specific adsorption of an osteopontin phosphopeptide. *J. Am. Chem. Soc*., 129, 14946-14951.

Harries J, Hukins D, Holt C. (1987). Conversion of amorphous calcium phosphate into hydroxyapatite. *J. Crystal Growth*, 84, 563-570.

Heughebaert J, Montel G (1982). Conversion of amorphous tricalcium phosphate into apatitic tricalcium phosphate. *Calcif .Tissue Int.*, 34, S103–8.

Hibi Y, Matsumoto T, Hagiwara S (1993). Effect of high pressure on the crystalline structure of various starch granules. *Cereal Chem*., 70, 671-676.

Hirsch A, Azuri I, Addadi L, Weiner S, Yang K, Curtarolo S, Kronik L (2014). Infrared absorption spectrum of brushite from first principles. *Chem. Mat.*, 26, 2934-2942.

Holt C, Timmins P, Errington N, Leaver J (1998). A core-shell model of calcium phosphate nanoclusters stabilized by β-casein phosphopeptides, derived from sedimentation equilibrium and small-angle X-ray and neutron-scattering measurements. *European J. Biochem.*, 252 (1), 73–78.

Holt C (1997). *The milk salts and their interaction with casein, in Advanced dairy chemistry, vol. 3: Lactose, water, salts and vitamins*, Chapman and Hall, London (Fox P, ed.), 233-256.

Holt C (2004). An equilibrium thermodynamic model of the sequestration of calcium phosphate by casein micelles and its application to the calculation of the partition of salts in milk. *European Bioph. J.,* 33, 421–434.

Holt C, Davies T, Law A (1986). Effects of colloidal calcium phosphate content and free calcium ion concentration in the milk serum on the dissociation of bovine casein micelles. *J. Dairy Research*, 6, 53, 557–572.

Holt C, Hasnain S, Hukins D (1982). Structure of bovine milk calcium phosphate determined by X-ray absorption spectroscopy. *Biochim. Biophys. Acta*, 719, 299–303.

Holt C, Hukins D (1991). Structural analysis of the environment of calcium ions in crystalline and amorphous calcium phosphates by x-ray absorption spectroscopy and a

hypothesis concerning the biological function of the casein micelle. *Int. Dairy Journal*, 1, 151–165.

Holt C, Lenton S, Nylander T, Sørensen E, Teixeira S (2014). Mineralisation of soft and hard tissues and the stability of biofluids. *J. Struct. Biology*, 185 (3), 383-396.

Holt C, Sørensen E, Clegg R (2009). Role of calcium phosphate nanoclusters in the control of calcification. *FEBS J.*, 276, 2308–23.

Holt C, van Kemenade CM, Nelson L, Sawyer L, Harries J, Bailey R, Hukins R (1989). Composition and structure of micellar calcium phosphate *J. Dairy Research*, 56, 411-416.

Holt C, Wahlgren N, Drakenberg T (1996). Ability of a beta-casein phosphopeptide to modulate the precipitation of calcium phosphate by forming amorphous dicalcium phosphate nanoclusters. *Biochem. J.*, 314, 1035–1039.

Hunter G, Hauschka P, Poole A, Rosenberg L, Goldberg H (1996). Nucleation and inhibition of hydroxyapatite formation by mineralized tissue proteins. *Biochem. J.*, 317, 59–64.

Kantoğlu Ö, Güven O (2002). *Nuclear Instruments and Methods in Physics Research Section B: Beam Interactions with Materials and Atoms*, 197, 3–4, 259-264.

Kojima Y, Sakama K, Toyama T, Yasue T, Arai Y (1994). Dehydration of water molecule in amorphous calcium phosphate. *Phosphorus Res. Bull.*, 4, 47–52.

Lee J, Ryu M, Baek H-R, Lee K, Seo J-H, Lee H-K (2013). Fabrication and evaluation of porous β-tricalcium phosphate/hydroxyapatite (60/40) composite as a bone graft extender using rat calvarial bone defect model. *The Scientific World Journal*, doi:10.1155/2013/481789.

Liu X, Hanson BL, Langan P, Viola RE (2007). The effect of deuteration on protein structure: a high-resolution comparison of hydrogenous and perdeuterated haloalkane dehalogenase. *Acta Cryst. D63*, 1000-1008.

Lyster R, Mann S, Parker S, Williams R (1984). The nature of micellular calcium phosphate in cows milk as studied by high resolution electron microscopy. *Biochim. Biophys. Acta*, 801, 315-317.

Mahamid J, Aichmayer B, Shimoni E, Ziblat R, Li C, Siegel S, Paris O, Fratzl P, Weiner S, Addadi L (2010). Mapping amorphous calcium phosphate transformation into crystalline mineral from the cell to the bone in zebrafish fin rays. *P.N.A.S. USA*, 107, 6316–6321.

Mahamid J, Sharir A, Gur D, Zelzer E, Addadi L, Weiner S (2011). Bone mineralization proceeds through intracellular calcium phosphate loaded vesicles: a cryo-electron microscopy study. *J. Struct. Biol.*, 174, 527–535.

McGann T, Buchheim W, Kearney R, Richardson T (1983). Composition and ultrastructure of calcium phosphate-citrate complexes in bovine milk systems. *Biochim. Biophys. Acta*, 760, 415–20.

Miller M, Kendall M, Jain M, Larson P, Madden A, Tas A (2012). Testing of brushite ($CaHPO_4 \cdot 2H_2O$) in synthetic biomineralization solutions and in situ crystallization of brushite micro-granules *J. Am. Ceram. Soc.*, 95, 2178–2188.

Mittemeijer E, Welzel U (2008). The “state of the art” of the diffraction analysis of crystallite size and lattice strain. *Z. Kristallogr.*, 223, 552–560.

Nelson D, McLean J (1984). High resolution electron microscopy of octacalcium phosphate and its hydrolysis products. *Calcif. Tissue Int.*, 36, 219-232.

Nudelman F, Bomans P, George A, De With G, Sommerdijk N (2012). The role of the amorphous phase on the biomimetic mineralization of collagen. *Faraday Discussions*, 159, 357-370.

Ono T, Ohotawa T, Tagaki Y (1994). Complexes of casein phosphopeptide and Calcium Phosphate prepared from Casein micelles by tryptic digestion. *Biosci. Biotech. Biochem*., 58, 1376-1380.

Paris O (2008). From diffraction to imaging: new avenues in studying hierarchical biological tissues with X-ray microbeams. *Biointerphases*, 3(2), FB16-26.

Perry P, Donald A (2000). The role of plasticization in starch granule assembly. *Int. J. Biological Macromolecules*, 28(1), 31-39.

Posner A, Perloff A, Diorio A (1958). Refinement of the hydroxyapatite structure. *Acta Crystallographica*, 11, 308-309

Rey C, Combes C, Drouet C, Sfihi H, Barroug A (2007). Physico-chemical properties of nanocrystalline apatites: implications for biominerals and biomaterials. *Materials Science and Engineering: C*, 27, 2, 198-205.

Reynolds E, Riley P, Adamson N (1994). A selective precipitation purification procedure for multiple phosphoseryl-containing peptides and methods for their identification.*Anal. Biochem*., 217, 277–284.

Richard D, Ferrand M, Kearley G (1996). Analysis and Visualisation of Neutron-Scattering Data. *J. Neutron Res.*, 4, 33–39 .

Rodriguez D, Thula-Mata T, Toro E, Yeh Y, Holt C, Holliday CL, Gower L (2014). Multifunctional role of osteopontin in directing intrafibrillar mineralization of collagen and activation of osteoclasts. *Acta Biomater*., 10, 494-507.

Rodriguez-Carvajal J (1993). Recent advances in magnetic structure determination by neutron powder diffraction. *Physica B*, 192, 55-69.

Rodriguez-Carvajal J. (2001). FullProf. 98 and WinPLOTR: New Windows 95/NT Applications for Diffraction. *Commission on Powder Diffraction, IUCr, Newsletter*, 26, 12-19.

Sarsfield B, Davidovich M, Desikan S, Fakes M, Futernik S, Hilden J, Tan J, Yin S, Young G, Vakkalagadda B, Volk K (2006). Powder X-ray diffraction detection of crystalline phases in amorphous pharmaceuticals. *JCPDS-International Centre for Diffraction Data*.

Skrtic D, Antonucci J, Eanes E (2003). Amorphous Calcium Phosphate-Based Bioactive Polymeric Composites for Mineralized Tissue Regeneration. *J. Res. Natl. Inst. Stand. Technol.* , 108, 167-182.

Thorn D, Meehan S, Sunde M, Rekas A, Gras S, MacPhee C, Dobson C, Wilson M, Carver J (2005). Amyloid fibril formation by bovine milk κ-casein and its inhibition by the molecular chaperones αS-and β-casein. *Biochemistry*, 44, 17027–17036.

Trpkovska M, Šoptrajanov B, Malkov P (1999). FTIR reinvestigation of the spectra of synthetic brushite and its partially deuterated analogues. *J. Mol. Structure*, 480-481, 661–666.

Yang Y, Kim K, Agrawal C, Ong J (2003). Effect of post-deposition heating time and the presence of water vapor during heat treatment on crystallinity of calcium phosphate coatings. *Biomaterials*, 24 (28), 5131-5137.

Zahid E, Lebugle A, Bonel G (1985). Sur une nouvelle classe de matériaux pour prothèses osseuses ou dentaires. *Bull. Soc. Chim. Fr.*, 4, 523–7.

Zhao J, Liu Y, Sun W, Zhang H (2011). Amorphous calcium phosphate and its application in dentistry. *Chem. Cent. J.*, 5, 40.

Supplementary Material – European Biophysics Journal

STRUCTURAL STUDIES OF HYDRATED SAMPLES OF AMORPHOUS CALCIUM PHOSPHATE AND PHOSPHOPEPTIDE NANOCLUSTERS

Samuel Lenton[a,b], Tommy Nylander[c], Carl Holt[d], Lindsay Sawyer[e], Michael Haertlein[b], Harrald Müller[f], Susana C.M. Teixeira[a,b]*

[a]EPSAM, Keele University, Staffordshire, ST5 5BG, UK. [b]Institut Laue–Langevin, 71 avenue des Martyrs – CS 20156, 38042 Grenoble cedex 9, France. [c]Dep. of Chemistry, Division of Physical Chemistry, Lund University, P.O. Box 124, S-221 00 Lund, Sweden. [d]Institute of Molecular, Cell and Systems Biology, University of Glasgow, Glasgow G12 8QQ, UK. [e]Structural Biochemistry Group, Michael Swann Building, The King's Buildings, University of Edinburgh, Mayfield Road, Edinburgh EH9 3JR, Scotland. [f]European Synchrotron Radiation Facility, CS 40220, 38043 Grenoble, France. *Corresponding author: Susana C.M. Teixeira, Tel. +33(0)675135513. Email: teixeira@ill.fr

FOURIER TRANSFORM INFRARED SPECTROSCOPY

Broad bands caused by the DCPD H-stretch of HPO_4 anions (Hadzi, 1965) are centred ~2900 cm^{-1}. DCPD shows a pair of doublets centered ~3480 cm^{-1} and ~3200 cm^{-1}, respectively, due to the O-H stretching modes of water. These are not visible for ACP or dry OPNmix CPN samples. The characteristic water bending mode (1649 cm^{-1}) and subsidiary peak (1730 cm^{-1}) are also clear in the DCPD spectrum but absent in the OPNmix CPN spectra (Figures S1 and S2).

The FTIR spectrum for ACP is in close agreement with the literature (Combes and Rey 2010), with broad phosphate stretching and bending modes and no apparent effects from the presence of bovine β-casein. The expected presence of adsorbed water is confirmed by the H-O-H bending modes and broadening of the 2500-3650 cm^{-1} band. The strong peak at 890 cm^{-1} was assigned to the P-O(H) stretch from protonated phosphate groups, absent in all CPN samples but presumably obscured by other absorption bands (in agreement with previously published results, see for example Miller 2012 or Holt et al. 1986).

This peak is consistent with the less stable ACP phase that converts to DCPD (Combes and Rey 2010), a result that is in agreement with the observed maturation of the ACP hydrated sample (see section 3.3 of main article) despite the presence of the crystallisation inhibitors.

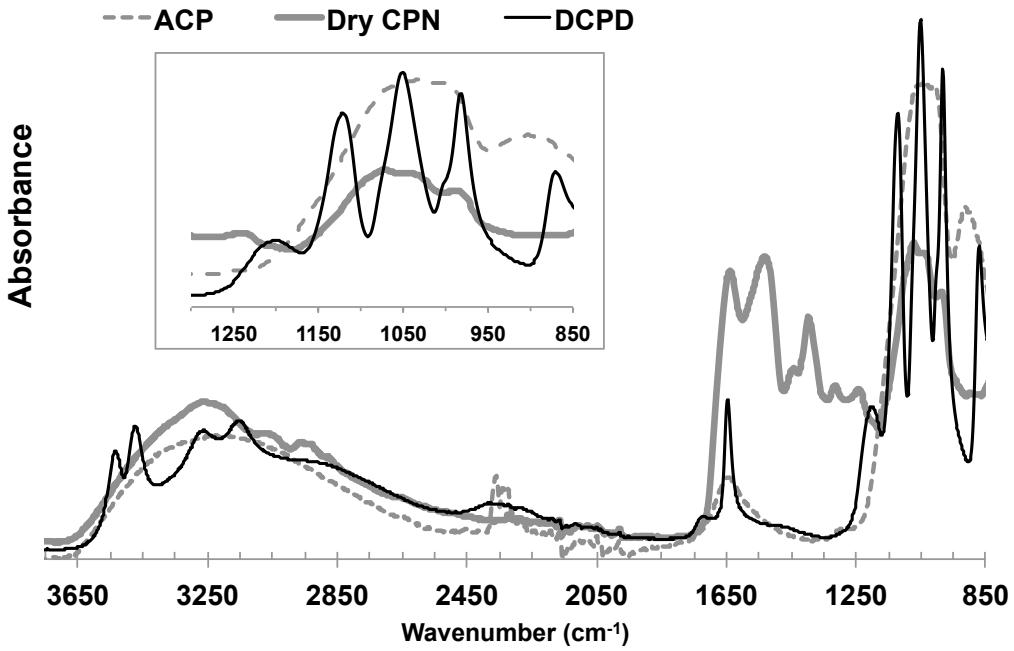

Figure S1. Overlay of FTIR spectra of dried samples: OPNmix CPN (dry CPN), DCPD and ACP. The inset shows the same spectra after Fourier self-deconvolution of the phosphate stretching region (850-1300 cm^{-1}). The expected lifting of the degeneracy of the broad phosphate asymmetric stretch (inset) and the phosphate bending mode (550cm^{-1}, data not shown) for crystalline calcium orthophosphates is clearly seen for DCPD but not for CPN or ACP samples. It should be noted that background peaks originating from the presence of atmospheric carbon dioxide (2350 cm^{-1}) and from the diamond (2000- 2100 cm^{-1}) anvils of the ATR-device are more obvious in the ACP spectrum due to the scale used.

The OPN protein backbone amide I and II bands (Gericke et al. 2005; Arrondo and Goni 1999) are clear for all CPN (see Figure S2), including micellar calcium phosphate (Gebhardt et al. 2011). The hydrated CPN samples also show enhanced absorbance at ~1645 cm^{-1}, where C=O group absorption in random coil, polyproline-II, or loop structures is expected, as well as water bending vibrations.

A strong peak at 1020 cm^{-1} and a broad peak at 1100 cm^{-1} are visible in the hydrated OPNmix CPN spectra, but not the OPNmix CPN dry spectrum. Bands at the same wavenumbers have been previously shown to occur in non-stoichiometric

apatites (Nudelman et al. 2012, Mahamid et al. 2010) containing hydrogen phosphate ions. The D-O-D (1150-1250 cm^{-1}) and D-O-H (1300-1550 cm^{-1}) bending modes are observed, as expected in the hydrated OPNmix CPN spectra (clearer for the 100% D_2O spectrum).

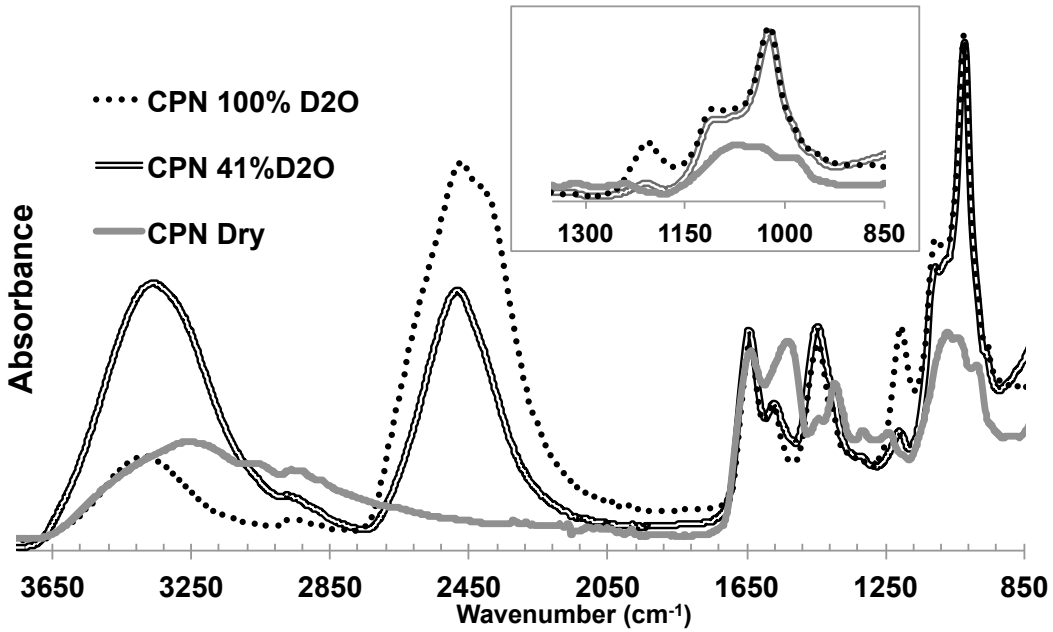

Figure S2. Overlay of FTIR spectra of OPNmix CPN. The inset shows the same spectra after Fourier self-deconvolution for the phosphate stretching region (850-1350 cm^{-1}). The intense broad bands at ~3400 cm^{-1} or 2500 cm^{-1} in the FTIR spectra of the hydrated samples are typical of structural OH and OD stretches, respectively, broadened by H/D bridging between water molecules.

Neutron and X-ray diffraction simulations

Diffraction patterns were simulated both for X-rays and neutrons using the Institut Laue-Langevin's PHP-MySQL Inorganic Crystal Structure Database (ICSD-for-WWW) using the Caglioti width parameters (Caglioti 1970, Hewat 1975): (0.05, -0.06, 0.07) for the Genix X-ray source. For D16 neutrons the parameters used were (0.5365, -0.4121, 0.355), calculated using the FullProf software suite (Rodriguez-Carvajal1993). Figure S3 shows the simulated patterns for angular detection ranges used for X-ray (S3a) and neutron (S3b) experimental data collection, where representative forms often studied or observed in biomaterials

were chosen. The crystal size was not taken into account for the simulations shown.

Figure S3 highlights the complementarity of the techniques, which allow for extended angular ranges to be covered while the respective technique sensitivities are fully explored. It is for example clear that even ignoring possible X-ray radiation damage effects, for OCP detection neutron diffraction can be more advantageous.

The DCPD structure has water molecules sandwiched between corrugated sheets of calcium and hydrogen phosphate ions. It typically yields a characteristic X-ray diffraction spectrum with strong reflections arising from these sheets (Figure S3a).

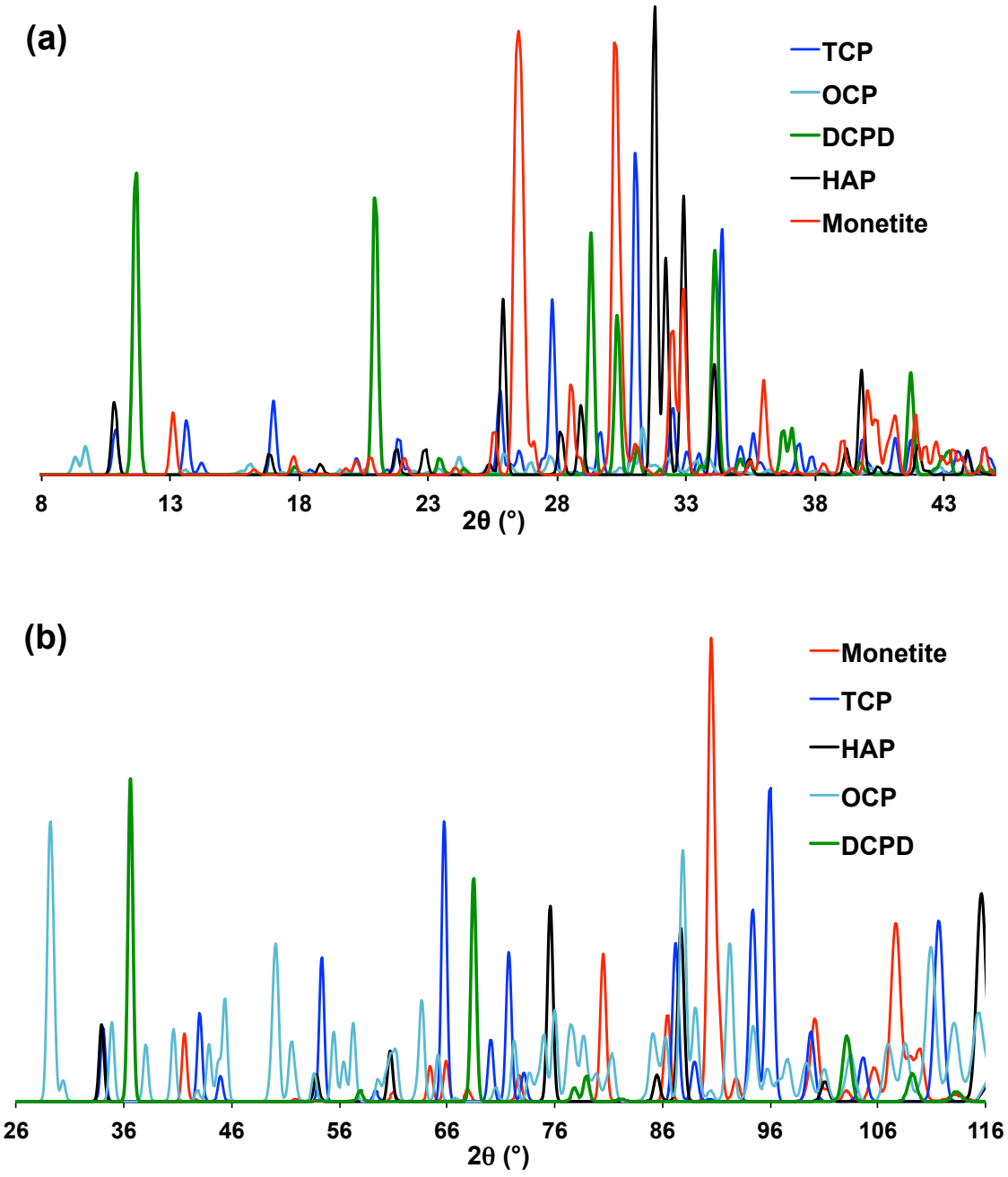

Figure S3. Calculated diffraction patterns for several different forms of calcium phosphate, based on previously published crystal structures of: primitive monetite (dicalcium phosphate anhydrous; Catti et al. 1980), β-TCP (Yashima et al. 2003), hexagonal HA (Posner et al. 1958), DCPD (Sainz-Díaz et al. 2004), and OCP (Brown 1962). The patterns were simulated for **(a)** X-rays of λ = 1.54Å and **(b)** neutrons of λ = 4.76Å.

References

Arrondo J, Goñi F (1999). Structure and dynamics of membrane proteins as studied by infrared spectroscopy. *Prog. Biophys. Mol. Biol.*, 72, 367-405.

Brown W (1962). Crystallographic and chemical relations between octacalcium phosphate and hydroxyapatite. *Nature*, 196, 1048-1050.

Caglioti G (1970). *Conventional and three-axis neutron powder diffraction, in Thermal Neutron Diffraction*, (Willis B, ed.), 0UP London, 14-33.

Catti M, Ferraris G and Mason S (1980). Low-temperature ordering of hydrogen atoms in CaHPO4 (monetite): X-ray and neutron diffraction study at 145 K. *Acta Cryst.*, B36, 254-259

Combes C, Rey C (2010). Amorphous calcium phosphates: Synthesis, properties and uses in biomaterials. *Acta Biomaterialia*, 6(9), 3362-3378.

Curry N and Jones D (1971). Crystal structure of brushite, calcium hydrogen orthophosphate dihydrate: a neutron-diffraction investigation. *J. Chem. Soc. A: Inorganic, Physical, Theoretical*, 3725-3729.

Gebhardt N, Takeda U, Kulozik U, Doster D (2011). Structure and stabilizing interactions of casein micelles probed by high-pressure light scattering and FTIR. *J. Phys. Chem. B*, 115, 2349–2359.

Gericke A, Qin C, Spevak L, Fujimoto Y, Butler W, Sørensen E, Boskey A (2005). Importance of phosphorylation for osteopontin regulation of biomineralization. *Calcif. Tissue Int.*, 77, 45–54.

Hadzi D (1965). Infrared spectra of strongly hydrogen-bonded systems. *Pure Applied Chem. J.*, 11, 435–454.

Hewat A (1975). Design for a conventional high resolution neutron powder diffractometer. *Nucl. Inst. Methods*, 127, 361-70.

Holt C, Davies T, Law A (1986). Effects of colloidal calcium phosphate content and free calcium ion concentration in the milk serum on the dissociation of bovine casein micelles. *J. Dairy Research*, 6, 53, 557–572.

Mahamid J, Aichmayer B, Shimoni E, Ziblat R, Li C, Siegel S, Paris O, Fratzl P, Weiner S, Addadi L (2010). Mapping amorphous calcium phosphate transformation into crystalline mineral from the cell to the bone in zebrafish fin rays. *P.N.A.S. USA*, 107, 6316–6321.

Miller M, Kendall M, Jain M, Larson P, Madden A, Tas A (2012). Testing of brushite ($CaHPO_4 \cdot 2H_2O$) in synthetic biomineralization solutions and in situ crystallization of brushite micro-granules *J. Am. Ceram. Soc.*, 95, 2178–2188.

Nudelman F, Bomans P, George A, De With G, Sommerdijk N (2012). The role of the amorphous phase on the biomimetic mineralization of collagen. *Faraday Discussions*, 159, 357-370.

Posner A, Perloff A and Diorio A (1958). Refinement of the hydroxyapatite structure. *Acta Cryst.*, 11, 308-309.

Rodriguez-Carvajal J (1993). Recent advances in magnetic structure determination by neutron powder diffraction. *Physica B*, 192, 1-2, 55-69.

Sainz-Díaz C, Villacampa A and Otálora F (2004). Crystallographic properties of the calcium phosphate mineral, Brushite, by means of First Principles Calculations. *American Mineralogist*, 89, 307-313.

Yashima M, Sakai A, Kamiyama T. and Hoshikawa A (2003). Crystal structure analysis of β-tricalcium phosphate $Ca_3(PO_4)_2$ by neutron powder diffraction. *J. Solid State Chem.*, 175, 272-277.